Technical University of Denmark

DTU

Upconversion detection of long-wave infrared radiation from a quantum cascade laser

Tseng, Yu-Pei; Pedersen, Christian; Tidemand-Lichtenberg, Peter

Link back to DTU Orbit

DTU Library
Technical Information Center of Denmark

Upconversion detection of long-wave infrared radiation from a quantum cascade laser

YU-PEI TSENG,* CHRISTIAN PEDERSEN, AND PETER TIDEMAND-LICHTENBERG

DTU Fotonik, Technical University of Denmark, Roskilde, 4000, Denmark
*yupts@fotonik.dtu.dk

Abstract: Broadly tunable upconversion is demonstrated for long-wave infrared (LWIR) detection. The upconversion system is evaluated by the detection of 50 ns pulses from a narrow linewidth tunable quantum cascade laser (QCL) in the 9.4 to 12 µm range. The LWIR signal is mixed with a 1064 nm laser beam in a silver gallium sulfide ($AgGaS_2$) crystal, resulting in an upconverted signal in the 956 to 977 nm range, using angle tuning for optimal phase-matching. This allows for efficient, high speed detection using a standard silicon detector. A theoretical model including absorption and diffraction shows qualitative agreement with experimental data.

OCIS codes: (190.0190) Nonlinear optics; (190.7220) Upconversion.

References and links

1. E. Normand, M. McCulloch, G. Duxbury, and N. Langford, "Fast, real-time spectrometer based on a pulsed quantum-cascade laser," Opt. Lett. **28**(1), 16–18 (2003).
2. D. D. Nelson, B. McManus, S. Urbanski, S. Herndon, and M. S. Zahniser, "High precision measurements of atmospheric nitrous oxide and methane using thermoelectrically cooled mid-infrared quantum cascade lasers and detectors," Spectrochim. Acta A Mol. Biomol. Spectrosc. **60**(14), 3325–3335 (2004).
3. M. Imaki and T. Kobayashi, "Infrared frequency upconverter for high-sensitivity imaging of gas plumes," Opt. Lett. **32**(13), 1923–1925 (2007).
4. P. Tidemand-Lichtenberg, J. S. Dam, H. V. Andersen, L. Høgstedt, and C. Pedersen, "Mid-infrared upconversion spectroscopy," J. Opt. Soc. Am. B **33**(11), D28–D35 (2016).
5. R. W. Boyd and C. H. Townes, "An infrared upconverter for astronomical imaging," Appl. Phys. Lett. **31**(7), 440–442 (1977).
6. M. R. Kole, R. K. Reddy, M. V. Schulmerich, M. K. Gelber, and R. Bhargava, "Discrete Frequency Infrared Microspectroscopy and Imaging with a Tunable Quantum Cascade Laser," Anal. Chem. **84**(23), 10366–10372 (2012).
7. N. Kröger, A. Egl, M. Engel, N. Gretz, K. Haase, I. Herpich, B. Kränzlin, S. Neudecker, A. Pucci, A. Schönhals, J. Vogt, and W. Petrich, "Quantum cascade laser-based hyperspectral imaging of biological tissue," J. Biomed. Opt. **19**(11), 111607 (2014).
8. K. Yeh, S. Kenkel, J. N. Liu, and R. Bhargava, "Fast Infrared Chemical Imaging with a Quantum Cascade Laser," Anal. Chem. **87**(1), 485–493 (2015).
9. P. Ciais, C. Sabine, G. Bala, L. Bopp, V. Brovkin, J. Canadell, A. Chhabra, R. DeFries, J. Galloway, M. Heimann, C. Jones, C. Le Qu'er'e, R. B. Myneni, S. Piao, and P. Thornton, "2013: Carbon and Other Biogeochemical Cycles," *in Climate Change 2013: The Physical Science Basis. Contribution of Working Group I to the Fifth Assessment Report of the Intergovernmental Panel on Climate Change*, Stocker, T. F. D. Qin, G. -K. Plattner, M. Tignor, S. K. Allen, J. Boschung, A. Nauels, Y. Xia, V. Bex and P. M. Midgley, eds. (Cambridge University, 2013).
10. Z. W. Sun, Z. S. Li, B. Li, M. Aldén, and P. Ewart, "Detection of C_2H_2 and HCl using mid-infrared degenerate four-wave mixing with stable beam alignment: towards practical in situ sensing of trace molecular species," Appl. Phys. B **98**(2-3), 593–600 (2010).
11. Y. Saalberg and M. Wolff, "VOC breath biomarkers in lung cancer," Clin. Chim. Acta **459**, 5–9 (2016).
12. E. van Mastrigt, A. Reyes-Reyes, K. Brand, N. Bhattacharya, H. P. Urbach, A. P. Stubbs, J. C. de Jongste, and M. W. Pijnenburg, "Exhaled breath profiling using broadband quantum cascade laser-based spectroscopy in healthy children and children with asthma and cystic fibrosis," J. Breath Res. **10**(2), 026003 (2016).
13. T. Stacewicz, Z. Bielecki, J. Wojtas, P. Magryta, J. Mikolajczyk, and D. Szabra, "Detection of disease markers in human breath with laser absorption spectroscopy," Opto-Electron. Rev. **24**(2), 82–94 (2016).
14. R. Baker, K. D. Rogers, N. Shepherd, and N. Stone, "New relationships between breast microcalcifications and cancer," Br. J. Cancer **103**(7), 1034–1039 (2010).

15. S. C. Kumar, P. G. Schunemann, K. T. Zawilski, and M. Eberahim-Zadeh, "Advances in ultrafast optical parametric sources for the mid-infrared based on $CdSiP_2$," JOSA B **33**, 44–56 (2016).
16. A. Hugi, R. Terazzi, Y. Bonetti, A. Wittmann, M. Fischer, M. Beck, J. Faist, and E. Gini, "External cavity quantum cascade laser tunable from 7.6 to 11.7μm," Appl. Phys. Lett. **2834**, 2007–2010 (2009)
17. A. Rogalski, *Infrared Detectors* (CRC Press, 2010).
18. J. S. Dam, C. Pedersen, and P. Tidemand-Lichtenberg, "Room temperature mid-IR single photon spectral imaging," Nat. Photonics **6**(11), 788–793 (2012).
19. G. Temporão, S. Tanzilli, H. Zbinden, N. Gisin, T. Aellen, M. Giovannini, and J. Faist, "Mid-infrared single-photon counting," Opt. Lett. **31**(8), 1094–1096 (2006).
20. L. Høgstedt, A. Fix, M. Wirth, C. Pedersen, and P. Tidemand-Lichtenberg, "Upconversion-based lidar measurements of atmospheric CO_2," Opt. Express **24**(5), 5152–5161 (2016).
21. Y.-P. Tseng, P. Bouzy, N. Stone, C. Pedersen, and P. Tidemand-Lichtenberg, "Long wavelength identification of microcalcifications in breast cancer tissue using a quantum cascade laser and upconversion detection," Proc. SPIE **1049**, 10490 (2018).
22. J.-J. Zondy, "The effects of focusing in type-I and type-II difference-frequency generations," Opt. Commun. **149**(1-3), 181–206 (1998).
23. K. Karstad, A. Stefanov, M. Wegmuller, H. Zbinden, N. Gisin, T. Aellen, M. Beck, and J. Faist, "Detection of mid-IR radiation by sum frequency generation for free space optical communication," Opt. Lasers Eng. **43**(3), 537–544 (2005).
24. G. D. Boyd and D. A. Kleinman, "Parametric Interaction of Focused Gaussian Light Beams," J. Appl. Phys. **39**(8), 3597–3639 (1968).
25. C. Pedersen, Q. Hu, L. Høgstedt, P. Tidemand-Lichtenberg, and J. S. Dam, "Non-collinear upconversion of infrared light," Opt. Express **22**(23), 28027–28036 (2014).
26. L. Wang, Z. Cao, H. Wang, H. Zhao, W. Gao, Y. Yuan, W. Chen, W. Zhang, Y. Wang, and X. Gao, "A widely tunable (5-12.5 μm) continuous-wave mid-infrared laser spectrometer based on difference frequency generation in $AgGaS_2$," Opt. Commun. **284**(1), 358–362 (2011).
27. E. Takaoka and K. Kato, "Thermo-optic dispersion formula for $AgGaS_2$," Appl. Opt. **38**(21), 4577–4580 (1999).

1. Introduction

Many substances can be identified by their spectral features associated with fundamental rotational and vibrational absorption bands in the infrared spectral region. This has spurred much attention to infrared (IR) technologies relating to applications, such as infrared spectroscopy [1–4] and infrared hyperspectral imaging [5–8]. Infrared spectroscopy has found applications within diverse fields like environmental gas monitoring [9,10] and medical applications e.g. exhaled breath analysis [11–13] and cancer diagnostics [14]. Throughout the past decades, significant scientific progress has led to new mid-IR light sources, such as narrow band optical parametric oscillators [15] and quantum cascade lasers (QCL's) [16]. Particularly the high efficiency, simple tuning properties and compact-size of QCL's has made it the ideal light source for many IR applications.

In contrast, there is a significant lack of low-noise infrared detectors [17] particularly at room temperature operation. Mercury cadmium telluride (MCT) detectors and bolometers are the standard choice for LWIR detection. However, direct LWIR detectors generally have poor signal-to-noise ratio, several orders of magnitude lower than that of silicon based detectors, mainly due to the unavoidable dark noise originating from the finite temperature of the detector. Cooling is therefore required to optimize the performance of traditional LWIR detectors, but it generally makes them bulky, expensive and inconvenient to use. Another issue is the response time of most direct LWIR detectors, which is generally much slower than their silicon counterpart. The lack of cheap, efficient detectors in the LWIR range has to some extent prevented widespread use of IR spectroscopy.

In recent years frequency upconversion has been revitalized as an alternative approach to direct detection of infrared radiation [18]. Upconversion relies on a nonlinear process commonly referred to as sum frequency generation, in which long wavelength (low energy) infrared photons are converted to near infrared (NIR) photons according to energy and momentum conservation when mixed with high energy photons from a laser field. This translates the IR signal to the NIR spectral range allowing for simple detection using silicon detectors. Most work on IR upconversion detection has been focused on the 1.5 to 4.5 μm range, where $LiNbO_3$ is the preferred nonlinear material [19,20]. However, moving beyond 5

µm little has been published on upconversion. In the LWIR range the selection of appropriate nonlinear crystals having high nonlinearity, high transmission in the LWIR and simultaneously at the upconverted wavelength range, combined with the ability to phase-match the nonlinear process, is very limited.

AgGaS$_2$ is becoming the nonlinear material of choice for upconversion based LWIR applications [2,4,21,22], since it is commercial available, has a fairly high nonlinear coefficient, d_{eff} ~16 pm/V and can be phase-matched over a broad range of wavelengths in the LWIR range, when mixing with lasers in the 1 µm range. In 2005 Karstad *et al.* demonstrated upconversion detection for free space communication at 9.3 µm using sum frequency generation of a LWIR QCL source and a 980 nm diode laser using AgGaS$_2$ as the nonlinear material [23]. Similarly AgGaS$_2$ has been used for non-collinear broadband LWIR upconversion spectroscopy in [4]. Moreover, Zondy *et al* demonstrated LWIR generation by difference frequency mixing of 778 and 843 nm using AgGaS$_2$ [22]. Generally the numerical simulations presented so far has not been very actuate in terms of power conversion efficiency considering parametric frequency conversion of focused LWIR Gaussian beams in AgGaS$_2$. Although AgGaS$_2$ has relatively low absorption loss below 8 µm, this is no longer the case in the 10 to 12 µm range. At longer wavelengths, absorption and diffraction become increasingly important to include in the modeling.

In this paper, we demonstrate upconversion detection of LWIR Gaussian beams from a QCL covering a wavelength range of 9.4 to 12 µm, using a silicon based detector to detect the upconverted signal. The influence of beam diffraction and LWIR absorption in the nonlinear material is analyzed experimentally and theoretically, showing nice agreement between simulations and measurements. We show in particular, the importance of including the angular dependence of the refractive index of the upconverted signal, when strong focusing is deployed. The performance of upconversion detection is evaluated in terms of efficiency, spectral coverage, acceptance parameters and speed, reaching an overall power conversion efficiency of the LWIR signal of more than 0.1% in the 10 µm spectral range using a 1064 nm mixing power of 3 W.

2. Experimental setup

The upconversion setup is illustrated in Fig. 1(a). A quantum cascade laser (Mini-QCL 100, BLOCK engineering) is used as a narrow linewidth LWIR source, widely tunable from 9.4 to 12 µm, delivering 50 ns pulses with a time separation of 1 µs. The normalized spectra and the output power of the tunable QCL source are shown in Fig. 1(b) and (c), respectively. The spectrum of the QCL was measured with a free-space coupled optical spectrum analyzer (OSA207C, Thorlabs). The linewidth of the QCL emission was found to be approx. 1 cm^{-1} for all wavelength settings. The mixing source is a diode pumped 1064 nm Nd:YVO$_4$ laser in continuous-wave operation delivering up to 3 W of output power. The sum frequency generation occurred in a 5 x 5 x 10 mm^3 AgGaS$_2$ crystal (High Technologies Laboratory, Kuban State University, Russia). The AgGaS$_2$ crystal was cut at θ = 43.3° (φ = 0) for type II phase-matching (e$_{ir}$ + o$_p$ → e$_{up}$).

The astigmatic output beam emitted from the QCL is circularized using two cylindrical ZnSe lenses of focal lengths, f$_1$ = 25.4 mm and f$_2$ = 50.8 mm, respectively. A half-wave plate (λ/2) is used to align the polarization of the LWIR radiation along the extraordinary axis of the nonlinear material. Two lenses of focal lengths, f$_3$ = 50 mm and f$_4$ = 150 mm, are used to focus the QCL and the mixing beam into the nonlinear crystal via a beam combiner. Both beams are focused in the center of the nonlinear crystal with a waist radius of approx. 100 µm. It is noted, that sum frequency generation gives a linear relationship between LWIR power and the upconverted signal power, where the conversion efficiency scales linearly with mixing power.

The AgGaS$_2$ crystal is mounted on a piezo controlled rotation stage (ECR3030, Attocube) for angle tuned birefringent phase-matching. The upconverted signal is collimated with a lens

of focal length, $f_5 = 75$ mm, filtered using a high reflection mirror at 1064 nm followed by three short-pass (SP 1000 nm) filters and a long-pass (LP 900 nm) filter, before being detected with a silicon detector.
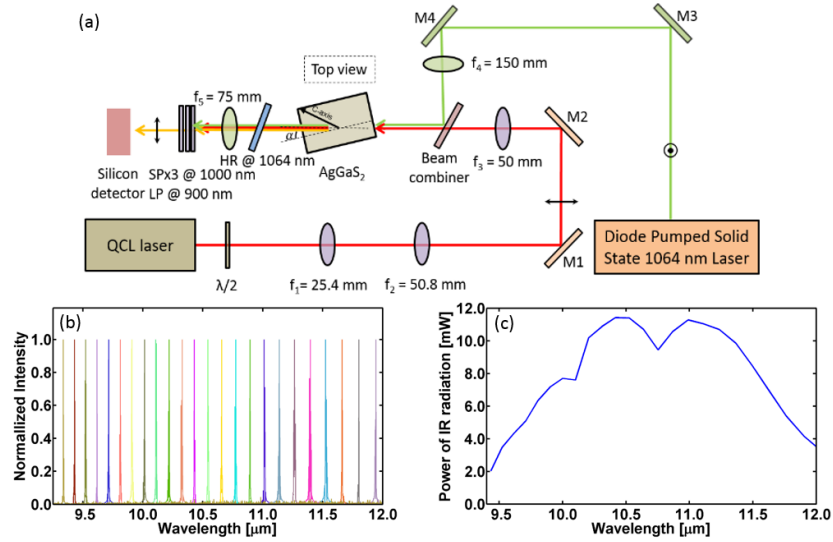

Fig. 1. (a) Schematic layout of experimental setup for upconversion detection. (b) Normalized spectral output of QCL at setting points from 9.35 µm (1070 cm⁻¹) to 11.9 µm (840 cm⁻¹) at ~120 nm (10 cm⁻¹) intervals. The different colors corresponds to different wavelength settings of the QCL laser. (c) Output power of QCL laser.

3. Theory

The simplest theoretical treatment of sum frequency generation relies on solving three coupled nonlinear differential equations, typically considering plane wave interaction of the three electromagnetic waves. However, particularly in the LWIR regime, it is important to take the finite beam size and diffraction into account even when working with moderately focused beams [22,24]. Approaching the transmission edge of the nonlinear material absorption also starts to play an important role, thus needs to be considered in order to accurately model the upconversion system.

The approach used here to evaluate the frequency conversion process is based on the far field solution of the Helmholtz equation assuming the small-signal approximation. In the following, the LWIR signal and the mixing field is assumed to propagate in the positive z-direction, having a Gaussian field distribution with beam waist w_i, wavelength λ_i, and a refractive index in the nonlinear material $n_i(\lambda_i, u, v)$, where "i" indicates the LWIR (ir), pump (p) and upconverted (up) field, respectively. u describes the propagation angle relative to the z-direction of the upconverted field in the plane of the optical axis (extraordinary plane), whereas v is the angle in the perpendicular direction (ordinary plane) relative to the z-direction [4]. Considering absorption only of the LWIR signal, the upconverted electric field (E_{up}) in the direction (u, v) at a distance r_{uv} can be expressed as [25]:

$$E_{up}\left(u,v,r_{uv}\right) = \frac{4\,d_{eff}\,\pi^2}{c\,\varepsilon_0\,\lambda_{up}^2} \cdot \frac{\exp\left(-i\,k_{up}\,r_{uv}\right)}{r_{uv}} \cdot \sqrt{\frac{2\cdot P_{ir}}{\pi\,n_{ir}\,w_{ir}^2} \cdot \frac{2\cdot P_p}{\pi\,n_p\,w_p^2}} \cdot \int_{l_1}^{l_2} \exp\left(-\frac{\alpha_{ir}}{2}\left(z+\frac{l}{2}\right)\right) \cdot$$

$$\frac{w_{ir}^2\,w_p^2}{w_{ir}^2 + i\frac{\lambda_{ir}z}{\pi n_{ir}} + w_p^2 + i\frac{\lambda_p z}{\pi n_p}} \cdot \exp\left(\frac{-\frac{1}{4}\left(w_{ir}^2 + i\frac{\lambda_{ir}z}{\pi n_{ir}}\right)\left(w_p^2 + i\frac{\lambda_p z}{\pi n_p}\right)}{w_{ir}^2 + i\frac{\lambda_{ir}z}{\pi n_{ir}} + w_p^2 + i\frac{\lambda_p z}{\pi n_p}}\left(\Delta k_u^2 + \Delta k_v^2\right)\right) \cdot \exp\left(i\,\Delta k_z\,z\right)dz$$

$$(1)$$

where α_{ir} is the absorption coefficient for the infrared radiation, $l = l_2 - l_1$ is the length of nonlinear crystal, r_{uv} is the distance from the source to the far field observation point. The phase-mismatch term Δk (vectorial) is evaluated according to the Sellmeier equations [26,27] of the nonlinear material, for a given propagation direction of the upconverted field given by (u, v). In Eq. (1), Δk has been separated into a longitudinal Δk_z and a transverse contribution Δk_T, where the transverse contribution relates to the finite beam size. Δk_u and Δk_v represents the transverse phase-mismatch term in u and v directions, respectively, as defined in [4]. The transverse mismatching term is often ignored in calculations of conversion efficiencies. The total upconverted power is found by integrating the absolute square of the upconverted field, $|E_{up}|^2$ with respect to u and v. Note that the refractive index n_{up} as well as the phase-mismatch Δk depends on the direction (u, v).

$$P_{up} = \frac{c\,\varepsilon_0\,n_{up}}{2} \iint\limits_{u,v} \left| E_{up}\left(u, v, r_{uv}\right) \right|^2 r_{uv}^2 \, du\, dv \qquad (2)$$

4. Results and discussion

In the following, the upconverted intensity distribution is evaluated based on Eq. (1), taking into account the influence of LWIR beam diffraction, and the birefringent nature of the nonlinear material giving a refractive index of the upconverted signal that depend on the direction of propagation. In the v-direction this gives a symmetric intensity distribution, however, in the u-direction this is no longer the case, as the angular dependent refractive index breaks the circular symmetry usually observed in upconverted signals. As a result the upconverted signal becomes elliptical or even breaks up into several loops, due to alternating constructive and destructive interference in the u-directions within the far-field angles of the upconverted signal.

Figure 2 contains arrays of upconverted images, showing both experimental and simulated intensity distributions at wavelengths of 10.0, 10.3, and 10.6 µm, respectively, for three crystal angles. For each wavelength the upconverted intensity distributions are shown for crystal rotation angles of −7.9, −8.8, and −9.6°, respectively, for the experimental images and for crystal rotation angles of −7.5, −8.4 and −9.2° for the simulated intensities. The images called 'central' in Fig. 2 are measured/simulated at optimum power conversion efficiency.

The upconverted power obtained at phase-matched crystal rotation angles are significantly larger than those obtained at non-optimal phase-matched angles. To compensate for this the integration time is adjusted accordingly so that for the 10 µm images an integration time of 5, 600, and 890 ms is used corresponding to rotation angles of −7.9 (optimal phase-matched angle), −8.8 and −9.6°, respectively. Rotating the crystal angle away from the optimal phase-matched condition, is seen to result in multi-lobed intensity profiles.
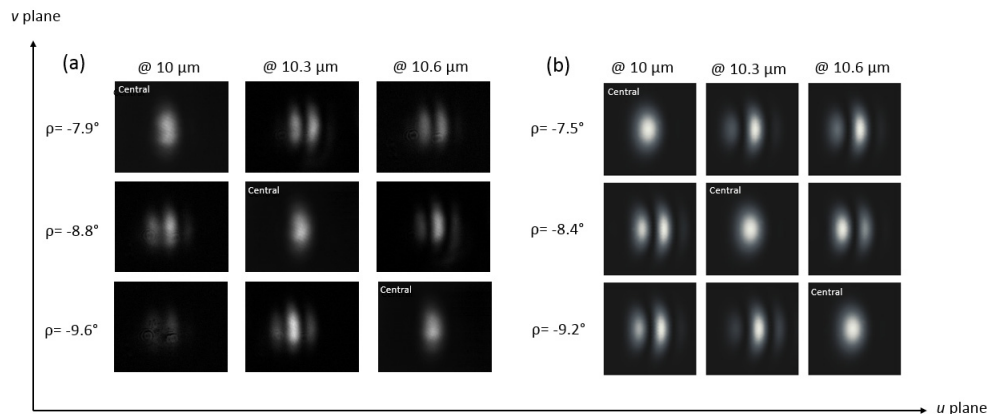
Fig. 2(a) Experimental images of upconverted signals detected with a Si-based camera at the crystal rotation angles of −7.9, −8.8, and −9.6° as the central (optimal phase-matched angles) obtained at the wavelengths of 10, 10.3, and 10.6 μm, respectively. (b) Simulated images of upconverted signal intensities at the crystal rotation angles of −7.5, −8.4, and −9.2° corresponding to the wavelengths of 10, 10.3, and 10.6 μm, respectively.

Figure 2(b) shows the simulated intensity distribution using Eq. (1) at 10, 10.3, and 10.6 μm, respectively. In order to maximize conversion efficiencies it was found, that the crystal rotation was off by 0.4° compared to the measurements for all images, this is likely be due to the experimental uncertainty of the actual crystal rotation angles used. In conclusion, we find good qualitative agreement between the measured intensity distribution and the simulated results using Eq. (1), hence, this model is used in the following sections to evaluate the efficiency and acceptance parameters of upconversion detection in the LWIR range.

Figure 3(a) shows the angle tuning of the phase-matching condition for upconversion of LWIR radiation. The wavelength range from 9.4 to 12 μm is upconverted to the NIR range (from 956 to 977 nm) by type II collinear phase-matching. The angle of the nonlinear crystal is optimized corresponding to optimal phase-matching (maximum power conversion efficiency) of the incident light. The upconverted signal is detected using a silicon detector. The Blue curve is calculated using a simple plane wave approach based on the Sellmeier equation found in [25,26]. The Red circles indicate the setting wavelength of the QCL at the angle giving maximum power, whereas the Black error bars indicate the wavelength shift between the setting point of the QCL and the measured wavelength using the OSA207C. The measured angles shows good agreement with the theoretical simulations.

The angular and wavelength acceptance bandwidths of the nonlinear frequency conversion process were investigated, as a measure of the accuracy needed in the phase-matching parameters to maximize conversion efficiency. Figure 3(b) shows the measured and the simulated conversion efficiencies as a function of rotation angle of the nonlinear material. The graphs have been normalized to accommodate the different conversion efficiencies obtained for the different numerical models. As seen later, from Fig. 4(a), the simulated efficiencies for focused Gaussian beams, including loss and an effective crystal length of 7.7 mm, taking beam walk-off into account, match the efficiency of the measured data.

The simulated results in Fig. 3(b) are obtained using Eq. (1) and (2). The LWIR wavelength was fixed at 10.3 μm and the upconverted signal was measured at each rotation angle of the nonlinear material using a silicon detector (S120C, Thorlabs). The measured full width half maximum bandwidth is ~0.4°. It is clearly seen, that the plane wave approximation is no longer valid (solid/dashed Blue lines, crystal lengths of 10 mm and 7.7 mm respectively) for $w_{ir} = w_p = 100$ μm due to diffraction of the LWIR beam. Taking the walk-off of the extraordinary polarized LWIR beam into account (ρ_{ir} ~23 mrad), an effective interaction length of 7.7 mm is found [24]. Simulated data for crystal lengths of 10 mm (solid Red line)

and 7.7 mm (dashed Red line) using Eq. (1) and (2) are shown in Fig. 3(b) considering the reduced interaction length. Good agreement is observed between the simulated (Red graph) and the measured (Red circles) data. Similar data are shown for the wavelength acceptance bandwidth at a fixed crystal rotation of −8.5° giving a full width half maximum wavelength acceptance bandwidth of 120 nm, see Fig. 3(c). Good agreement is found between the measured data and the simulated graph obtained using integral theory.

Figure 4(a) shows the upconverted power as a function of LWIR wavelength. The Blue graph is calculated using the wavelength dependent QCL power as input, using a plane wave approximation with 10 mm interaction length, without LWIR absorption in the nonlinear material. The dotted (without crystal absorption) and solid/dashed (with crystal absorption) Red lines are simulated using Eq. (1) and (2) with the interaction lengths of 10 mm and 7.7 mm, respectively. Red circles are experimental data, measuring the upconverted power with a silicon power meter for optimized crystal rotation. The filter losses on upconverted power are taken into account. With the used focusing parameters it is interesting to note, that the power conversion scales approx. linear with crystal length. Optimizing the phase mismatch to accommodate for the Gouy phase-shift increase the conversion efficiency by approx. 3% compared to $\Delta k = 0$ (optimal for plane wave interaction). This optimization of phase mismatch is important to align the center wavelength of the acceptance graphs of Fig. 3, as it shifts the crystal rotation angle by 0.05 degree or the phase matched wavelength by 15 nm.
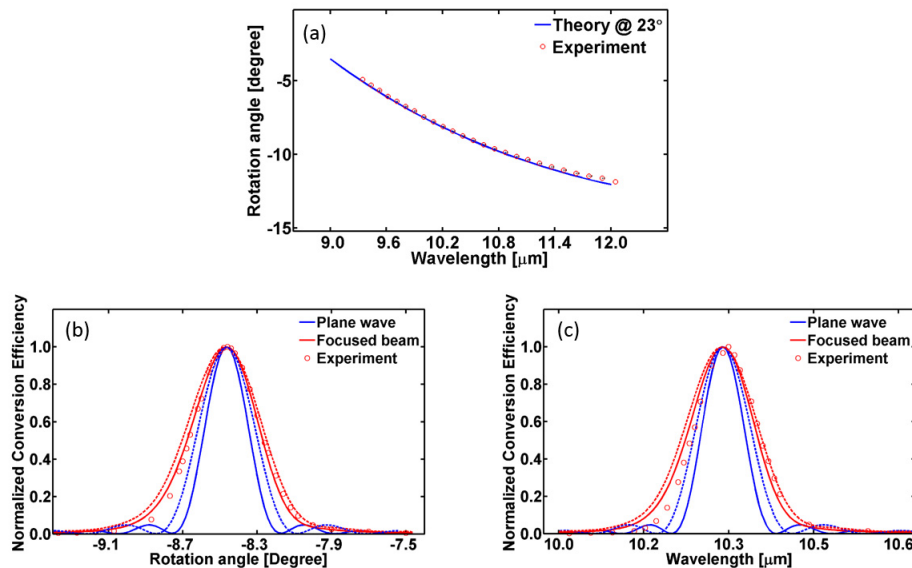

Fig. 3(a) Phase-matching angle tuning versus wavelength of long-wave infrared from 9.4 µm to 12 µm at ~120 nm (10 cm-1) intervals. (b) Conversion efficiency versus crystal rotation angle at a wavelength of 10.3 µm. The angles calculated using plane wave theory were shifted by 0.05 degree. (c) Wavelength acceptance bandwidth at −8.5° crystal rotation angle. The wavelengths calculated using plane wave theory were shifted by 15 nm.

The system was aligned at an LWIR wavelength of $\lambda_{ir} = 10.3$ µm, giving a maximum measured upconverted power of ~2.2 µW for a fixed mixing power of 320 mW (Reduced power is used to minimize thermal effects in the nonlinear material). As the crystal is rotated for optimum phase-matching for the different QCL wavelengths, the refractive index difference of the two fields reduce the spatial overlap, resulting in a decreased upconverted efficiency when tuning away from 10.3 µm. Furthermore, it was observed that both beam pointing stability and mode quality of the QCL laser degraded as it was tuned towards long wavelengths, leading to reduced conversion efficiency. The measured upconversion

efficiency as a function of mixing power at 10.3 µm is illustrated in Fig. 4(b), showing a linear increase in the conversion efficiency with increasing pump power. AgGaS$_2$ has poor thermal conductivity, meaning that thermal lensing becomes an increasing issue as the mixing power is increased, leading to reduced accuracies in theoretical modeling, see Fig. 4(b).
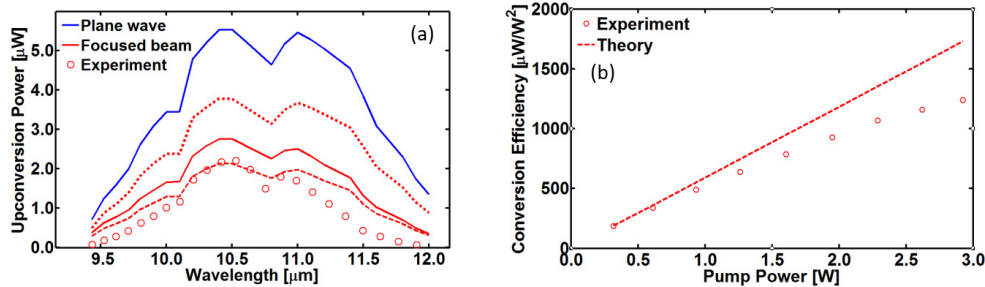

Fig. 4(a) Experimental (Red circles) and theoretical upconversion powers in terms of plane wave approximation based non-absorbed (Blue curve) at 10 mm crystal length and focused infrared beam based on integral theory at the crystal lengths of 10 mm, dotted (non-absorbed) and (with absorption) Red curves. The dashed Red (with absorption) curve shows simulated upconverted power at 7.7 mm crystal length based on integral theory. (b) Experimental conversion efficiency (Red circles) as a function of pump power at a given infrared power. The dashed Red line shows conversion efficiency calculated at IR power of 10.47 mW and a 7.7 mm interaction length using integral theory.

Direct detection of LWIR pulses has traditionally been challenging due to a slow rise time of MCT detectors. Upconversion allows for the use of silicon detectors typically having much faster response time. Figure 5(a) shows typical oscilloscope traces of upconverted LWIR pulses with a duration of 50 ns (λ_{ir} = 10.3 µm). The upconverted signal is detected by a silicon avalanche photodiode (APD210, Thorlabs) having a rise time of 500 ps, showing good signal to noise ratio even for single pulse detection. The average power of the LWIR signal is varied between 10.22 and 5.24 mW, adjusting the QCL driving current.

Figure 5(b) shows oscilloscope traces averaged by 50 sweeps and enlarged time scale in order to visualize the pulse separation of 1 µs. It should be noted that pulse shape is tilted due to the AC coupled mode of operation of the APD detector. Using a stable continuous-wave pump laser for the upconversion process, the frequency conversion scheme does not add timing jitter nor amplitude fluctuations to the upconverted signals, hence, allowing for direct pulse characterization.
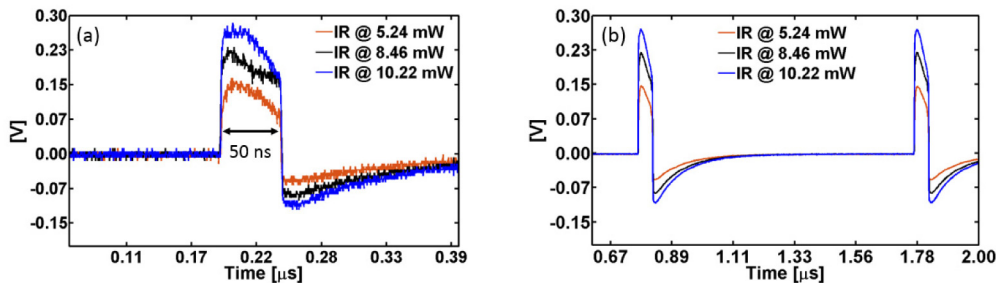

Fig. 5. (a) Oscilloscope traces of upconverted signals, at IR power of 5.24, 8.48, and 10.22 mW respectively. (b) Oscilloscope traces of upconverted signals averaged by 50 sweeps.

5. Conclusion

In this paper, we demonstrate the potential of upconversion detection for long-wave infrared sensing in a wide wavelength range, demonstrating fast acquisition speed of LWIR pulses,

with good signal-to-noise ratio even for single pulse detection, suitable for real life applications at room temperature operation. Long-wave infrared signals were successfully upconverted to the near infrared range allowing for detection using fast, efficient and low-noise silicon detectors. The fast acquisition time has potential for real-time measurement. A detailed numerical model was presented, showing excellent agreement with measured data, both in terms of conversion efficiencies and acceptance parameters, taking into account the finite beam sizes, diffraction and absorption of the infrared signal in the nonlinear crystal. Such detailed analysis paves the way for upconversion detection used for raster scanned imaging in the LWIR range. The absorption of the $AgGaS_2$ crystal increases dramatically above 8 µm, nevertheless it is still possible to use this material for upconversion detection up to about 12 µm if the losses are properly accounted for in the simulations. The obtained result shows great potential for upconversion detection in long-wave infrared spectroscopy.